International Journal of Heat and Mass Transfer 131 (2019) 772–780

Contents lists available at ScienceDirect

International Journal of Heat and Mass Transfer

journal homepage: www.elsevier.com/locate/ijhmt

A hyperbolic lattice Boltzmann method for simulating non-Fourier heat conduction

Yi Liu, Ling Li *, Qin Lou

School of Energy and Power Engineering, University of Shanghai for Science and Technology, Shanghai 200093, China

ARTICLE INFO

Article history:
Received 10 August 2018
Received in revised form 1 November 2018
Accepted 22 November 2018
Available online 28 November 2018

Keywords:
Hyperbolic lattice Boltzmann method
Dual phase lag model
Non-Fourier heat conduction

ABSTRACT

Classical lattice Boltzmann method (LBM) can recover Fourier's law. Since Fourier's law results in a parabolic heat conduction equation, the classical LBM is called the parabolic Boltzmann method (PLBM). But the Fourier's law is based on the absurd assumption that the heat transfer rate is infinite, so whether the classical LBM can be used to observe the non-Fourier heat transfer problem remains controversial. In this paper, a hyperbolic lattice Boltzmann method (HLBM), which can be used to analyze the non-Fourier effect, was derived based on the Cattaneo-Vernotte (CV) model. To verify the accuracy of the HLBM, the process of a gold film irradiated by the laser was simulated using the HLBM and the PLBM and the results were compared with the experimental data. Because of the non-equilibrium heat transfer between electron and lattice during the laser irradiation, the two-step HLBM/PLBM models were proposed according to the two-temperature model. The results show that the electron temperatures simulated by the two models are not much different from each other, and both of them coincide with the experimental values. However, the thresholds obtained by the two models are different, and the results of HLBM are closer to the experimental values.

1. Introduction

Fourier proposed the famous Fourier heat conduction law in *the Analytical Theory of Heat* [1], and then the law was widely used to solve macroscopic heat conduction problem [2]. However, the Fourier heat conduction law is based on the absurd assumption that the heat transfer rate is infinite [3]. Therefore in some special cases such as very short time, high heat fluxes and ultra-low temperature, the propagation speed of heat wave cannot be simply regard as infinite, the Fourier's law may not be valid anymore [4]. In addition, Fourier's law is summarized by steady-state heat conduction experiments, so it is controversial whether it can be directly extended to an unsteady state. To improve Fourier's law, Cattaneo [5,6] and Vernotte [7] introduced the concept of relaxation time τ based on the assumption that heat transfer rate is limited. The expression of τ_q is α/c_h^2, α is the thermal diffusion coefficient and c_h is the propagation speed of heat wave. The model proposed by Cattaneo and Vernotte is called the CV model. The physical meaning of the CV model is that a temperature gradient is generated at the time t and at the position x, then a heat flow vector is generated there, but the heat fluxes vector is generated at time $t+\tau_q$ instead of time t, which is different from Fourier's law. From the point of view of the partial differential equation, a hyperbolic equation can be obtained by CV model, while a parabolic equation can be derived by Fourier model. Therefore, the problem of heat conduction considering the non-Fourier effect is called a hyperbolic heat conduction problem [3,8].

The CV model has been widely used in the discussion of heat conduction phenomena in the fields of medicine [9], laser [10,11] and thermal shock fracture [12]. Most of them use the macroscopic models and finite difference methods. The advantage of the macro method is that a simple mathematical formula can describe a phenomenon, but it cannot explain the microscopic mechanism. Molecular dynamics is a commonly used microscopic method. In contrast to macroscopic methods, molecular dynamics can reflect the microscopic mechanism of a phenomenon, but it requires a lot of calculations, and for some relatively large systems, distortion may occur. The mesoscopic method is a method proposed in recent years, which can be considered as a combination of macro method and micro method [13,14]. The lattice Boltzmann method (LBM) is a commonly used mesoscopic method, which has three advantages [14,15]: (1) based on the Boltzmann equation, which satisfies the molecular kinetic theory; (2) easy to implement parallel operations; and (3) easy to handle complex geometric boundaries. LBM is a special numerical solution method for the Boltzmann equation

* Corresponding author.
E-mail address: liling@usst.edu.cn (L. Li).

https://doi.org/10.1016/j.ijheatmasstransfer.2018.11.110
0017-9310/

Nomenclature

B_e	coefficient for electron heat capacity, $J/\left(m^3 \cdot K^2\right)$
c	velocity vector
C	heat capacity, J/K
C_e	heat capacity of electron, J/K
$C_{p,l}$	specific heat of lattice, $J/(kg \cdot K)$
c_s	sound speed, m/s
e	internal energy, J
f_i	distribution function of temperature
g_i	distribution function of internal energy
G	electron-lattice coupling coefficient, $W/(m^2 \cdot K)$
G_0	A function of Temperature
J	heat source fluence, J/m^2
J_{th}	damage threshold, J/m^2
k	thermal conductivity, $W/(m \cdot K)$
L	thickness of the metal film, m
M	dimensionless standard deviation
R	reflectivity
S, S^*	intensity of the internal heat source, W/m^3
t	time, s
T	temperature, K
T_F	Fermi temperature, K
t_p	pulse width, s
w_i	weighting factors
x	coordinate, m

Greek symbol

α	thermal diffusion coefficient, m^2/s
δ	optical penetration depth, m
δ_b	ballistic range, m
ε	Knudsen number
ρ	density, kg/m^3
τ_g	dimensionless relaxation factor
τ_q	relaxation time of heat flux, s
Λ	new collision operator

Superscript

0	last time step
eq	equilibrium state

Subscripts

e	electron
l	lattice

[16,17], which has been widely used in micro-/nanoscale flow [18] and multiphase flow [19] and so on.

At present, the LBM algorithm commonly used internationally is the LBM-BGK format proposed by Qian et al. [20] based on the BGK approximation [21]. This method is simple, while Bhatnagar et al. did not discuss the impact of the non-Fourier effect when proposing the BGK approximation, therefore, when discuss the non-Fourier effect by using LBM requires a second thought. Ho et al. [22] proposed an LB equation based on the dual-phase-lag (DPL) heat conduction model. They define the distribution function f_i as the product of the partial derivative of temperature over time and the heat flow relaxation time, i.e.

$$\tau_q \frac{\partial T}{\partial t} = \sum f_i(x,t) \tag{1}$$

This method is very simple in structure and is widely used [23,24]. While, it is a scheme for indirectly solving the temperature field, which is somewhat different from the feature that LBM can directly solve the partial differential equation. After more than ten years, Li et al. [25] also proposed an expanded lattice Boltzmann method (ELBM) based on the DPL model. The scheme can directly solve the temperature field, and the physical meaning is clear. But it didn't explore the source item, which will make the model more universal. In addition, when the DPL heat conduction equation with the source term is brought into the law of conservation of energy, it is not only simply to add a source term to the original equation, but there is also an additional item. This item is the product of the change rate of the source term over time and the heat flow relaxation time. The ELBM just combined a collision operator obtained based on a DPL model with a classical LBM. It didn't realize that the effect of relaxation time on the source term can also be included in the collision operator. The ELBM's processing of the source term still needs to be combined with the finite difference method (FDM), which is the same as the method of Ho et al. [22].

In this paper, based on the classical lattice Boltzmann method, a hyperbolic lattice Boltzmann method (HLBM) is proposed. Then HLBM and PLBM are used respectively to describe a typical non-Fourier heat transfer phenomenon of a gold film irradiated by ultra-short laser. The results of two models were analyzed and compared with the experimental data.

2. Derivation of HLBM

2.1. Classical lattice Boltzmann model

The equilibrium internal energy distribution function of the diffusion equation is $g_i^{eq} = w_i \rho e$, which should satisfy the following constraints

$$\sum_i g_i^{eq} = \rho e \tag{2}$$

$$\sum_i c_i g_i^{eq} = 0 \tag{3}$$

$$\sum_{i,j} c_i c_j g_i^{eq} = pe\delta_{ij} = pe \tag{4}$$

where p is pressure, $p = c_s^2 \rho$, ρ is density, e is internal energy, w_i is weighting factor, c_i is velocity vector and c_s is the sound speed.

The latticed Boltzmann equation (LBE) of internal energy is

$$g_i(x + \Delta x, t + \Delta t) - g_i(x,t) = -\frac{1}{\tau_g}\left[g_i(x,t) - g_i^{eq}(x,t)\right] \tag{5}$$

where τ_g is the dimensionless relaxation factor which represents the collision frequency between molecules, and $g_i(x,t)$ is the distribution function of internal energy. Introduce the Chapman-Enskog expansions [13]:

$$\frac{\partial}{\partial t} = \varepsilon \frac{\partial}{\partial t_1} + \varepsilon^2 \frac{\partial}{\partial t_2} \tag{6}$$

$$\frac{\partial}{\partial x} = \varepsilon \frac{\partial}{\partial x_1} \tag{7}$$

where ε is the Knudsen number. Eq. (5) can rewritten as

$$\left(\frac{\partial}{\partial t_1}+c_i\frac{\partial}{\partial x_1}\right)g_i^{eq}+\frac{1}{\tau_g}g_i^{(1)}=0 \tag{8}$$

$$\frac{\partial g_i^{eq}}{\partial t_2}+\left(1-\frac{1}{2\tau_g}\right)\left(\frac{\partial}{\partial t_1}+c_i\frac{\partial}{\partial x_1}\right)g_i^{(1)}+\frac{1}{\tau_g}g_i^{(2)}=0 \tag{9}$$

we can obtain the following two equations by Eq. (8).

$$\frac{\partial(\rho e)}{\partial t_1}=0 \tag{10}$$

$$\begin{aligned} c_i g_i^{(1)} &= -\tau_g\left(c_i\frac{\partial}{\partial t_1}+c_i c_i\frac{\partial}{\partial x_1}\right)g_i^{eq} \\ \Rightarrow \sum_i c_i g_i^{(1)} &= -\tau_g\sum_i\left(c_i\frac{\partial}{\partial t_1}+c_i c_i\frac{\partial}{\partial x_1}\right)g_i^{eq} \\ &= -\tau_g\frac{\partial}{\partial x_1}\left(\sum_i c_i c_i g_i^{eq}\right)=-\tau_g\frac{\partial(pe)}{\partial x_1}=-\tau_g\frac{\partial(c_s^2\rho e)}{\partial x_1} \end{aligned} \tag{11}$$

Sum the left and right sides of Eq. (9) and combine Eq. (3)

$$\frac{\partial(\rho e)}{\partial t_2}+\left(1-\frac{1}{2\tau_g}\right)\frac{\partial}{\partial x_1}\left(\sum_i c_i g_i^{(1)}\right)=0 \tag{12}$$

Substitute Eq. (11) into Eq. (12)

$$\frac{\partial(\rho e)}{\partial t_2}=\tau_g\left(1-\frac{1}{2\tau}\right)\frac{\partial}{\partial x_1}\left[\frac{\partial}{\partial x_1}\left(c_s^2\rho e\right)\right] \tag{13}$$

Then Eq. (10) × ε + Eq. (13) × ε^2

$$\frac{\partial e}{\partial t'}=\frac{\partial}{\partial x}\left(\tau_g c_s^2\frac{\partial e}{\partial x}\right) \tag{14}$$

Eq. (14) is the energy conservation equation. According to kinetic theory

$$\tau_g c_s^2 c_v=\tau_g c_g^2 c_v/3=\lambda \tag{15}$$

So $c_s^2=\frac{1}{3}v_g^2$, the result is consistent with the conclusion of Guo [26]. Therefore, the CV model cannot be obtained from the LBM.

2.2. Hyperbolic lattice Boltzmann method

When CV model inserted into the energy equation, a hyperbolic equation can be obtained [27]

$$C\tau_q\frac{\partial^2 T}{\partial t^2}+C\frac{\partial T}{\partial t}=\frac{\partial}{\partial x}\left(k\frac{\partial T}{\partial x}\right)+S+\tau_q\frac{\partial S}{\partial t} \tag{16}$$

In order to make the problem more general, we make $S=G_0+S^*$, i.e.

$$C\tau_q\frac{\partial^2 T}{\partial t^2}+C\frac{\partial T}{\partial t}=\frac{\partial}{\partial x}\left(k\frac{\partial T}{\partial x}\right)+G_0T+S^*+G_0\tau_q\frac{\partial T}{\partial t}+\tau_q\frac{\partial S^*}{\partial t} \tag{17}$$

G_0 is a function of T. By changing the form of Eq. (17), we can obtain

$$\frac{\partial T}{\partial t}=\frac{\alpha}{1+\tau_q\frac{\partial}{\partial t}}\frac{\partial^2 T}{\partial x^2}+\frac{G}{C}T+\frac{S^*}{C} \tag{18}$$

The LBM form of Eq. (18) as follow

$$\begin{aligned} &f_i(x+\Delta x,t+\Delta t)-f_i(x,t) \\ &=\Lambda\left[f_i(x,t)-f_i^{eq}(x,t)\right]+\frac{w_i\Delta t}{C}S_i^*+\frac{G_0}{C}f_i(x,t) \end{aligned} \tag{19}$$

Λ is the collision operator which we need. $f_i(x,t)$ is the distribution function of temperature, and $f_i^{eq}(x,t)$ is the equilibrium distribution function of temperature. We use the Taylor series of $f_i(x+\Delta x,t+\Delta t)$ about (x,t)

$$\begin{aligned} f_i(x+\Delta x,t+\Delta t) &= f_i(x,t)+\left(\frac{\partial}{\partial x}\Delta x+\frac{\partial}{\partial t}\Delta t\right)f_i \\ &\quad+\frac{1}{2}\left(\frac{\partial}{\partial x}\Delta x+\frac{\partial}{\partial t}\Delta t\right)^2 f_i \\ &= f_i+\frac{\partial f_i}{\partial x}\Delta x+\frac{\partial f_i}{\partial t}\Delta t+\frac{1}{2}\frac{\partial^2 f_i}{\partial x^2}(\Delta x)^2 \\ &\quad+\frac{1}{2}\frac{\partial^2 f_i}{\partial t^2}(\Delta t)^2+\frac{\partial^2 f_i}{\partial x\partial t}\Delta x\Delta t+\cdots \end{aligned} \tag{20}$$

So

$$\begin{aligned} &\Lambda\left[f_i(x,t)-f_i^{eq}(x,t)\right]+\frac{w_i\Delta t}{C}S_i^*+\frac{G_0\Delta t}{C}f_i(x,t) \\ &=\frac{\partial f_i}{\partial x}\Delta x+\frac{\partial f_i}{\partial t}\Delta t+\frac{1}{2}\frac{\partial^2 f_i}{\partial x^2}(\Delta x)^2+\frac{1}{2}\frac{\partial^2 f_i}{\partial t^2}(\Delta t)^2+\frac{\partial^2 f_i}{\partial t\partial x}\Delta x\Delta t \end{aligned} \tag{21}$$

Introducing Knudsen number ε [13]

$$\frac{\varepsilon^2}{\partial t}=\frac{1}{\partial t},\quad \frac{\varepsilon}{\partial x}=\frac{1}{\partial x} \tag{22}$$

then we obtained

$$\begin{aligned} &\Lambda\left[f_i-f_i^{eq}\right]+\varepsilon^2\frac{w_i\Delta t}{C}S_i^*+\varepsilon^2\frac{G_0\Delta t}{C}f_i(x,t) \\ &=\varepsilon\frac{\partial f_i}{\partial x}\Delta x+\varepsilon^2\frac{\partial f_i}{\partial t}\Delta t+\frac{1}{2}\varepsilon^2\frac{\partial^2 f_i}{\partial x^2}(\Delta x)^2+\mathrm{O}(\varepsilon^3) \end{aligned} \tag{23}$$

the Taylor expansion of $f_i(x,t)$ is

$$f_i=f_i^{(0)}+\varepsilon f_i^{(1)}+\varepsilon^2 f_i^{(2)} \tag{24}$$

where $f_i^{(0)}=f_i^{eq}$, $f_i^{(1)}$ and $f_i^{(2)}$ is the first-order and second-order derivative of $f_i^{(0)}$. We perform second-order perturbation expansion on S_i^* and G_0, i.e.

$$S_i^*=\varepsilon^2 S_i^* \tag{25}$$

$$G_0=\varepsilon^2 G_0 \tag{26}$$

therefor

$$\begin{aligned} &\Lambda\left[\varepsilon f_i^{(1)}+\varepsilon^2 f_i^{(2)}\right]+\varepsilon^2\frac{w_i\Delta t}{C}S_i^*+\varepsilon^2\frac{G_0\Delta t}{C}f_i(x,t) \\ &=\varepsilon\frac{\partial f_i^{(0)}}{\partial x}\Delta x+\varepsilon^2\frac{\partial f_i^{(1)}}{\partial x}\Delta x+\varepsilon^2\frac{\partial f_i^{(0)}}{\partial t}\Delta t+\frac{1}{2}\varepsilon^2\frac{\partial^2 f_i^{(0)}}{\partial x^2}(\Delta x)^2 \end{aligned} \tag{27}$$

According to the order of ε, we can rewrite the Eq. (27) as follow

$$\varepsilon:\frac{\partial f_i^{(0)}}{\partial x}\Delta x=\Lambda f_i^{(1)} \tag{28}$$

$$\begin{aligned} &\varepsilon^2:\frac{\partial f_i^{(1)}}{\partial x}\Delta x+\frac{\partial f_i^{(0)}}{\partial x}\Delta t+\frac{1}{2}\frac{\partial^2 f_i^{(0)}}{\partial x^2}(\Delta x)^2 \\ &=\Lambda f_i^{(2)}+\frac{w_i\Delta t}{C}S_i^*+\frac{G_0\Delta t}{C}f_i^{(0)} \end{aligned} \tag{29}$$

Calculating the gradient of Eq. (28)

$$\Lambda\frac{\partial f_i^{(1)}}{\partial x}=\frac{\partial^2 f_i^{(0)}}{\partial x^2}\Delta x \tag{30}$$

Inserting Eq. (30) into Eq. (29)

$$\frac{\partial f_i^{(0)}}{\partial t}\Delta t+\left(\frac{1}{2}+\frac{1}{\Lambda}\right)\frac{\partial^2 f_i^{(0)}}{\partial x^2}(\Delta x)^2=\Lambda f_i^{(2)}+\frac{w_i\Delta t}{C}S_i^*+\frac{G_0\Delta t}{C}f_i^{(0)} \tag{31}$$

Because

$$\sum_i f_i^{(0)}=T,\quad \sum_i f_i^{(1)}=\sum_i f_i^{(2)}=0,\quad \sum_i w_i S_i^*=S^* \tag{32}$$

so by summing all i in the Eq. (31), we can obtain

$$\frac{\partial T}{\partial t}+\frac{(\Delta x)^2}{\Delta t}\left(\frac{1}{2}+\frac{1}{\Lambda}\right)\frac{\partial^2 T}{\partial x^2}=\frac{S^*}{C}+\frac{G_0 T}{C} \tag{33}$$

Now we introduce two time operators Z^{-1} and Y

$$f_i(x,t-\Delta t)=Z^{-1}f_i(x,t) \tag{34}$$

$$\frac{\partial f_i(x,t)}{\partial t}=Yf_i(x,t) \tag{35}$$

By Taylor expansion, we know

$$f_i(x,t-\Delta t)=f_i(x,t)-\frac{\partial f_i(x,t)}{\partial t}\Delta t \tag{36}$$

in other words

$$Z^{-1}=1-Y\Delta t \tag{37}$$

In addition, Eq. (18) can be rewritten

$$\frac{\partial T}{\partial t}-\frac{\alpha}{1+\tau_q Y}\frac{\partial^2 T}{\partial x^2}=\frac{S^*}{C}+\frac{G_0}{C}T \tag{38}$$

Comparing Eq. (38) with Eq. (33), we can make a conclusion

$$\frac{1}{2}+\frac{1}{\Lambda}=-\frac{\Delta t}{(\Delta x)^2}\frac{\alpha}{1+\tau_q Y}=-\frac{\alpha^*}{1+\tau_q Y} \tag{39}$$

Solving Eq. (39)

$$\Lambda=-\frac{2(1+\tau_q Y)}{1+\tau_q Y+2\alpha^*} \tag{40}$$

insert Eq. (37) into Eq. (40)

$$\Lambda=-\frac{2\left[1+\frac{\tau_q}{\Delta t}\left(1-Z^{-1}\right)\right]}{1+\frac{\tau_q}{\Delta t}\left(1-Z^{-1}\right)+2\alpha^*} \tag{41}$$

we set $\Gamma=\tau_q/\Delta t$, then

$$\Lambda=-\frac{2\left[1+\Gamma\left(1-Z^{-1}\right)\right]}{1+\Gamma\left(1-Z^{-1}\right)+2\alpha^*} \tag{42}$$

Substitute Eq. (42) into Eq. (19)

$$f_i(x+\Delta x,t+\Delta t)-f_i(x,t)=-\frac{2\left[1+\Gamma\left(1-Z^{-1}\right)\right]}{1+\Gamma\left(1-Z^{-1}\right)+2\alpha^*}\left[f_i(x,t)-f_i^{eq}(x,t)\right]+\frac{w_i\Delta t}{C}S_i^*+\frac{G_0\Delta t}{C}f_i(x,t) \tag{43}$$

We set

$$\Psi_i(x,t)=f_i(x+\Delta x,t+\Delta t)-f_i(x,t) \tag{44}$$

$$\Theta_i(x,t)=f_i(x,t)-f_i^{eq}(x,t) \tag{45}$$

Then

$$\Psi_i=-\frac{2\left[1+\Gamma\left(1-Z^{-1}\right)\right]}{1+\Gamma\left(1-Z^{-1}\right)+2\alpha^*}\Theta_i+\frac{w_i\Delta t}{C}S_i^*+\frac{G_0\Delta t}{C}f_i(x,t)\Rightarrow\Psi_i$$
$$=\frac{\Gamma Z^{-1}\Psi_i-2(1+\Gamma)\Theta_i+2\Gamma Z^{-1}\Theta_i}{2\alpha^*+1+\Gamma}+\frac{w_i\Delta t}{C}S_i^*-\frac{w_i\Delta t}{C}\frac{\Gamma Z^{-1}S_i^*}{2\alpha^*+1+\Gamma}$$
$$+\frac{G_0\Delta t}{C}f_i(x,t)-\frac{G_0\Delta t}{C}\frac{\Gamma Z^{-1}f_i(x,t)}{2\alpha^*+1+\Gamma} \tag{46}$$

according to the definition of time operators

$$Z^{-1}\Psi_i(x,t)=\Psi_i(x,t-\Delta t)=\Psi_i^0 \tag{47}$$

$$Z^{-1}\Theta_i(x,t)=\Theta_i(x,t-\Delta t)=\Theta_i^0 \tag{48}$$

$$Z^{-1}S_i^*(x,t)=S_i^*(x,t-\Delta t)=S_i^{*,0} \tag{49}$$

we have

$$\Psi_i=\frac{\Gamma\Psi_i^0-2(1+\Gamma)\Theta_i+2\Gamma\Theta_i^0}{2\alpha^*+1+\Gamma}+\frac{w_i\Delta t}{C}S_i^*+\frac{G_0\Delta t}{C}f_i-\frac{w_i\Delta t}{C}\times\frac{\Gamma S_i^{*,0}}{2\alpha^*+1+\Gamma}-\frac{G_0\Delta t}{C}\frac{\Gamma f_i^0}{2\alpha^*+1+\Gamma} \tag{50}$$

Now we introduce two simplified coefficients for making the physical meaning of the Eq. (50) clearer.

$$\phi=\frac{\Gamma}{2\alpha^*+1+\Gamma} \tag{51}$$

$$\varphi=\frac{1}{2\alpha^*+1+\Gamma} \tag{52}$$

Finally, Eq. (50) can be rewritten as

$$\Psi_i-\phi\Psi_i^0=-2(\varphi+\phi)\Theta_i+2\phi\Theta_i^0+\frac{G_0\Delta t}{C}\left(f_i-\phi f_i^0\right)+\frac{w_i\Delta t}{C}\left(S_i^*-\phi S_i^{*,0}\right) \tag{53}$$

Since Eq. (53) can be reduced to a hyperbolic equation, we call Eq. (53) a hyperbolic lattice Boltzmann method (HLBM). When $\Gamma=0$, $\phi=0$, $\varphi=1/(2\alpha^*+1)$, at which time Eq. (53) degenerates into a classical LBM-BGK format (PLBM) that can be reduced to a parabolic equation:

$$\Psi_i=-2\varphi\Theta_i+\frac{G_0\Delta t}{C}f_i+\frac{w_i\Delta t}{C}S_i^* \tag{54}$$

3. The simulation of ultrashort laser heating materials using the HLBM

With the gradual improvement of LBM theory, the LBM method has also been applied to the field of laser processing [28]. When the metal material is irradiated with laser, if the time of the laser pulse is less than or equal to the equilibrium time of the electron and the phonon, the electrons and the lattices in the film may be in the unbalanced state [29]. In order to describe the non-equilibrium effect between electron and lattice temperature, the former Soviet scholar Anisimovsi et al. [30] proposed an electron-lattice two-temperature model (TTM) to explain this phenomenon. The model consists of two Fourier heat conduction equations with coupling terms. Since the Fourier heat conduction law is a parabolic equation, the model is also called the parabolic two-temperature model. Subsequently, Qiu and Tien [11] discovered from the Boltzmann equation that the two-temperature equation has a hyperbolic effect. They introduce the CV model into the two temperature model and propose a hyperbolic two-step model. Inspired by the predecessors, this paper proposes a two-step HLBM/PLBM model for the characteristics of the process.

3.1. Physical model

As shown in Fig. 1(a), the top of the gold film is irradiated by a laser beam. Since the thickness L of the gold film is much smaller than the width of the laser, this problem can be considered as a one-dimensional heat conduction problem. The coordinate system is established at the bottom of the gold film as the origin. The distribution of energy with time and space is shown in Fig. 1(b). The energy density of the laser is J, the pulse width is t_p. The energy of the laser obeys a Gaussian distribution with a mean of 0 and a variance of $t_p/\sqrt{8ln2}$. When the laser passes through the gold film, the distribution of the laser energy in the gold film satisfies Bouguer's

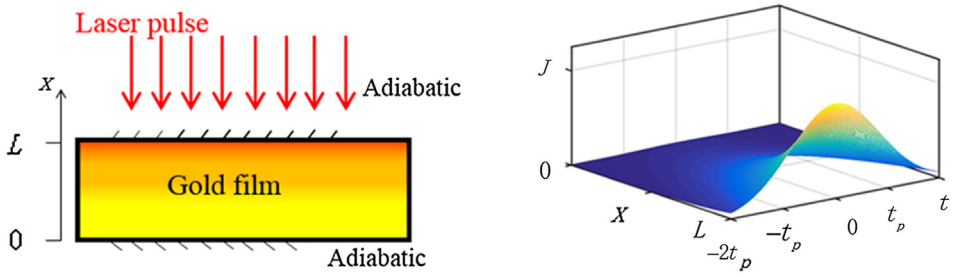

Fig. 1. Physical model. (a) Schematic diagram of laser irradiation on gold film. (b) Space-time distribution map of laser energy. The coordinate J represents the energy density of the laser. The coordinate t represents time. The laser energy obeys the Gaussian distribution in time with the initial time $-2t_p$. The ordinate L represents the thickness of film, where the laser energy satisfies the exponential distribution spatially.

law, that is, the radiant energy decays exponentially along the transfer path.

The initial condition for the problem is:

$$T_e = T_l = 300\ \mathrm{K} \quad t = -2t_p \tag{55}$$

Since the CV model is introduced in the energy conservation equation, the second derivative of time appears in the energy equation, so an extra time condition is required:

$$\frac{\partial T_e}{\partial t} = \frac{\partial T_l}{\partial t} = 0 \quad t = -2t_p \tag{56}$$

In the process of irradiating the surface of the gold film with ultra-short pulse laser, since the heat loss of the surface can be neglected [31], the surface can be regarded as an adiabatic surface, therefore the boundary condition is an adiabatic boundary condition:

$$\frac{\partial T_e}{\partial x} = \frac{\partial T_l}{\partial x} = 0 \quad x = 0, x = L \tag{57}$$

According to Eq. (53), the HLBM equation of two temperature model can be written as:

$$\Psi_{e,i} - \phi_e \Psi^0_{e,i} = -2(\varphi_e + \phi_e)\Theta_{e,i} + 2\phi_e \Theta^0_{e,i} + \frac{w_i \Delta t}{C_e}\left(S_i - \phi_e S^0_i\right) - \frac{G\Delta t}{C_e}\left[\left(f_{e,i} - \phi_e f^0_{e,i}\right) - \left(f_{l,i} - \phi_e f^0_{l,i}\right)\right] \tag{58}$$

$$\Psi_{l,i} - \phi_l \Psi^0_{l,i} = -2(\varphi_l + \phi_l)\Theta_{l,i} + 2\phi_l \Theta^0_{l,i} + \frac{G\Delta t}{C_l}\left[\left(f_{e,i} - \phi_l f^0_{e,i}\right) - \left(f_{l,i} - \phi_l f^0_{l,i}\right)\right] \tag{59}$$

$$\phi_e = \frac{\Gamma_e}{2\alpha^*_e + 1 + \Gamma_e}, \quad \varphi_e = \frac{1}{2\alpha^*_e + 1 + \Gamma_e} \tag{60}$$

$$\phi_l = \frac{\Gamma_l}{2\alpha^*_l + 1 + \Gamma_l}, \quad \varphi_l = \frac{1}{2\alpha^*_l + 1 + \Gamma_l} \tag{61}$$

The electronic heat capacity C_e can be obtained by [32]

$$C_e = \begin{cases} B_e T_e & T_e < T_F/\pi^2 \\ 2B_e T_e/3 + C'_e/3 & T_F/\pi^2 \leqslant T_e < 3T_F/\pi^2 \\ Nk_B + C'_e/3 & 3T_F/\pi^2 \leqslant T_e < T_F \\ 3Nk_B/2 & T_e \geqslant T_F \end{cases} \tag{62}$$

where

$$C'_e = B_e T_F/\pi^2 + \frac{3Nk_B/2 - B_e T_F/\pi^2}{T_F - T_F/\pi^2}\left(T_e - T_F/\pi^2\right) \tag{63}$$

The electronic thermal conductivity k_e is [33]

$$k_e = \chi \frac{\left(\vartheta_e^2 + 0.16\right)^{5/4}\left(\vartheta_e^2 + 0.44\right)\vartheta_e}{\left(\vartheta_e^2 + 0.092\right)^{1/2}\left(\vartheta_e^2 + \eta\vartheta_l\right)} \tag{64}$$

where $\vartheta_e = T_e/T_F$ and $\vartheta_l = T_l/T_F$.

From the Ref. [29], we know the coupling coefficient G is

$$G = G_{RT}\left[\frac{A_e}{B_l}(T_e - T_l) + 1\right] \tag{65}$$

where G_{RT} is the coupling coefficient at room temperature, A_e and B_l are material constant.

As for the role of laser, it can be regard as a source term S [34]

$$S = 0.94\frac{1-R}{t_p(\delta + \delta_b)\left[1 - e^{-L/(\delta+\delta_b)}\right]}J \times \exp\left[-\frac{L-x}{\delta+\delta_b} - 2.77\left(\frac{t}{t_p}\right)^2\right] \tag{66}$$

where J is the energy density of the laser, R is the reflectivity, δ is the optical penetration depth, δ_b is the ballistic range, and t_p is the pulse width.

The specific heat and thermal conductivity of lattices are [35]

$$C_{p,l} = 105.1 + 0.294T_l - 8.731 \times 10^{-4}T_l^2 + 1.187 \times 10^{-6}T_l^3 - 7.051 \times 10^{-10}T_l^4 + 1.538 \times 10^{-13}T_l^5 \tag{67}$$

$$k_{eq} = 320.973 - 0.0111T_l - 2.747 \times 10^{-5}T_l^2 - 4.048 \times 10^{-9}T_l^3 \tag{68}$$

$$k_l = 0.01k_{eq} \tag{69}$$

Fig. 2 is a flow chart of the HLBM-TTM algorithm. The algorithm consists of three cyclic processes: a main loop process (from step 3 to step 13) for calculating the temperature field evolution over time and two iterative loop processes (from step 3 to step 6, from step 7 to step 10) for calculating the spatial distribution of electrons and lattice temperatures, respectively. These two iterative cycles for calculating the electron and lattice temperatures are also referred to as inner loops, which are embedded in the main loop. The core of the algorithm is step 4 and step 8, we used HLBM to calculate the temperature of electron and lattice. The HLBM consists of two steps, one is the collision process and the other is the streaming process. The streaming process of HLBM is exactly the same as that of PLBM, but the collision process of HLBM uses the hyperbolic collision operator proposed in this paper, which is different from the classic PLBM. The specific steps of the algorithm are as follows:

Step 1: The required parameters are input. The specific parameters are detailed in Table 1.

Step 2: The initial parameters are set as:

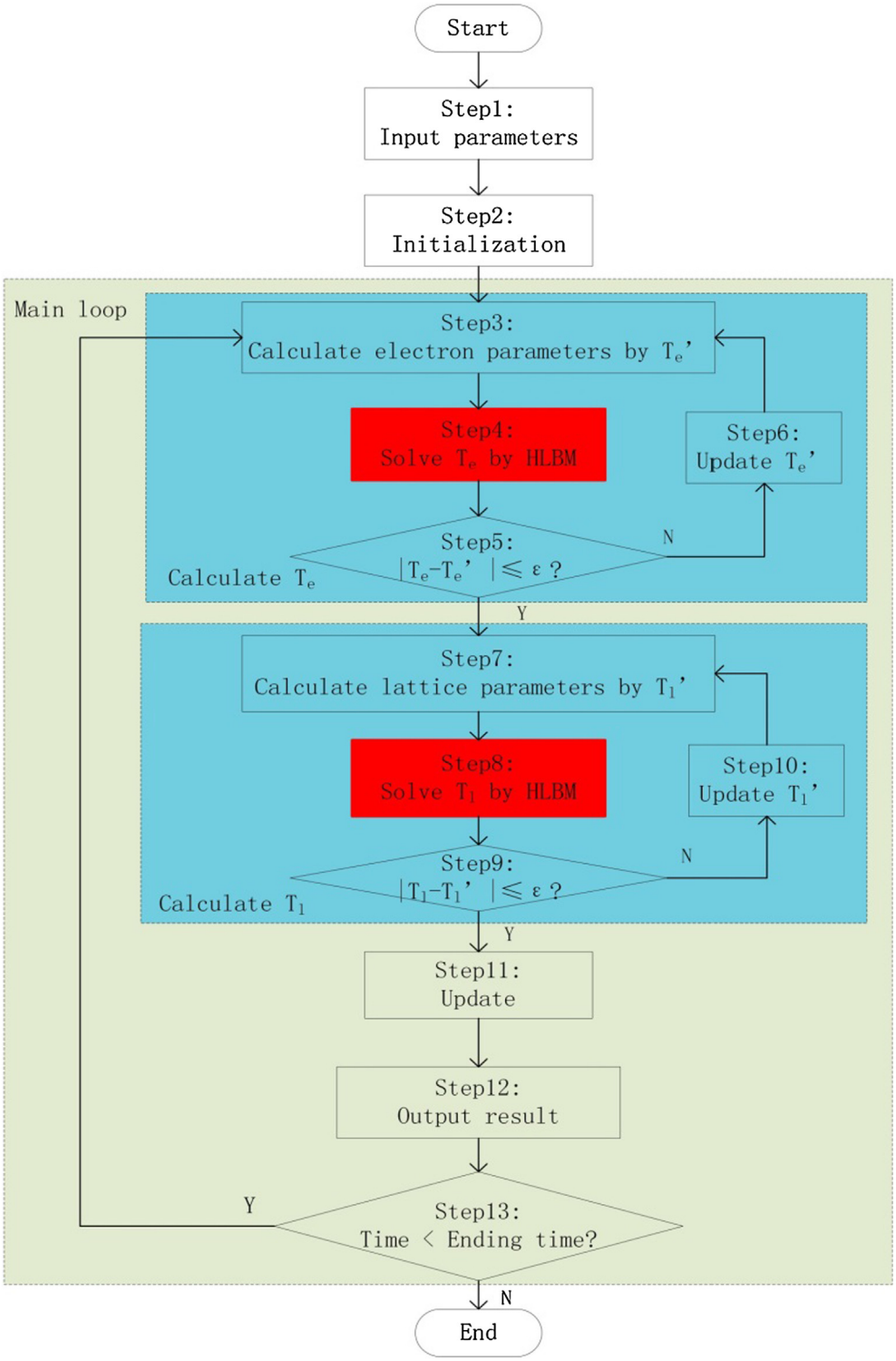

Fig. 2. Flow chart of HLBM-TTM. The green area is the external main loop process and is the evolution of temperature over time. The blue region is an iterative calculation process for electron and lattice temperatures, which is the evolution of temperature with space. The red area is the core of the algorithm, which is the process of solving the temperature field by HLBM. (For interpretation of the references to color in this figure legend, the reader is referred to the web version of this article.)

$$T_e = T_l = T_e^0 = T_l^0 = 300\ \mathrm{K} \tag{70}$$

$$f_{e,i}(x,t) = 0.5 \times T_e \quad f_{l,i}(x,t) = 0.5 \times T_l \tag{71}$$

$$f_{e,i}^{eq}(x,t) = 0.5 \times T_e \quad f_{l,i}^{eq}(x,t) = 0.5 \times T_l \tag{72}$$

$$f_{e,i}(x,t-\Delta t) = 0.5 \times T_e^0 \quad f_{l,i}(x,t-\Delta t) = 0.5 \times T_l^0 \tag{73}$$

$$f_{e,i}^{eq}(x,t-\Delta t) = 0.5 \times T_e^0 \quad f_{l,i}^{eq}(x,t-\Delta t) = 0.5 \times T_l^0 \tag{74}$$

$$\Psi_{e,i}^0 = \Psi_{l,i}^0 = 0 \quad S^0 = 0 \tag{75}$$

Table 1
Required parameters (except for special instructions, the rest of the parameters are from Ref. [35]).

Parameters	Unit	
Material constant, A_e		1.2×10^7
Material constant, B_l		1.23×10^{11}
Coefficient for electronic heat capacity, B_e		70
Coupling coefficient at room temperature, G_{RT}	W/(m^3·K)	2.2×10^{16}
Density, ρ	kg/m^3	19.3×10^3
Optical penetration depth, δ	nm	20.6
Fermi temperature, T_F	K	6.42×10^4
Coefficient for electronic conductivity, χ	W/(m·K)	353
Electronic relaxation time, τ_e	fs	40 [39]
Lattice relaxation time, τ_l	fs	800 [39]

Step 3: A hypothetical electron temperature T_e' is used to calculate the thermal physical parameters of the electron. In this step, the electronic heat capacity C_e, the electronic thermal conductivity k_e, the value of coupling coefficient G and the source term can be calculated by Eqs. (62), (64), (65) and (66), respectively.
Step 4: The governing equation of the electron temperature is solved through HLBM to obtain a pseudo real-time temperature T_e. This step is one of the core steps of the algorithm using HLBM to calculate the temperature field of electron. This step also can be divided into two steps: the collision progress and the streaming progress.

The collision progress is

$$\Psi_{e,i}(x,t) = f_{e,i}(x,t+\Delta t) - f_{e,i}(x,t) \tag{76}$$

$$\Psi_{e,i} - \phi_e \Psi^0_{e,i} = -2(\varphi_e + \phi_e)\Theta_{e,i} + 2\phi_e \Theta^0_{e,i} + \frac{w_i \Delta t}{C_e}\left(S_i - \phi_e S^0_i\right) - \frac{G\Delta t}{C_e}\left[\left(f_{e,i} - \phi_e f^0_{e,i}\right) - \left(f_{l,i} - \phi_e f^0_{l,i}\right)\right] \tag{77}$$

$$\Psi^0_{e,i}(x,t) = f_{e,i}(x,t) - f_{e,i}(x,t-\Delta t) \tag{78}$$

$$\Theta_{e,i} = f_{e,i}(x,t) - f^{eq}_{e,i}(x,t) \tag{79}$$

$$\Theta^0_{e,i} = f_{e,i}(x,t-\Delta t) - f^{eq}_{e,i}(x,t-\Delta t) \tag{80}$$

for D1Q2, $f^{eq}_{e,i}(x,t) = \frac{1}{2}T_e$.

The streaming progress is

$$f_{e,i}(x+\Delta x, t+\Delta t) = f_{e,i}(x,t+\Delta t) \tag{81}$$

The boundary conditions are

$$f_{e,i}(x=0,t) = f_{e,i}(x=\Delta x,t) \tag{82}$$

$$f_{e,i}(x=L,t) = f_{e,i}(x=L-\Delta x,t) \tag{83}$$

Step 5: Whether the absolute value of T_e-T_e' is less than ε or not is judged. If it's true, go to step 7, otherwise continue to step 3 after executing step 6, and repeat the progress until the judgment condition is satisfied. The value of ε is 10^{-8}, which is a small number used to determine whether T_e converges.
Step 6: T_e' is updated with the following formula

$$T_e' = T_e' + 0.5 \times (T_e - T_e') \tag{84}$$

Step 7: A hypothetical lattice temperature T_l' is used to calculate the thermal physical parameters of the lattice. The specific heat capacity $C_{p,l}$ and thermal conductivity k_l of the lattice are obtained by Eq. (67) and Eq. (69), respectively.

Step 8: The governing equation of the lattice temperature is solved through HLBM to obtain a pseudo real-time temperature T_l. This step is another core of the algorithm and it is basically the same as Step 4, except that the collision algorithm is slightly different. The collision process is

$$\Psi_{l,i} - \phi_l \Psi^0_{l,i} = -2(\varphi_l + \phi_l)\Theta_{l,i} + 2\phi_l \Theta^0_{l,i} + \frac{G\Delta t}{C_l}\left[\left(f_{e,i} - \phi_l f^0_{e,i}\right) - \left(f_{l,i} - \phi_l f^0_{l,i}\right)\right] \tag{85}$$

$$\Psi_{l,i}(x,t) = f_{l,i}(x,t+\Delta t) - f_{l,i}(x,t) \tag{86}$$

$$\Psi^0_{l,i}(x,t) = f_{l,i}(x,t) - f_{l,i}(x,t-\Delta t) \tag{87}$$

Step 9: Whether the absolute value of T_l-T_l' is less than ε or not is judged. If it's true, go to step 11, otherwise continue to step 7 after executing step 10, and repeat the progress until the judgment condition is satisfied.
Step 10: T_l' is updated with the following formula

$$T_l' = T_l' + 0.5 \times (T_l - T_l') \tag{88}$$

Step 11: Functions are updated. We have

$$f_i(x,t-\Delta t) = f_i(x,t) \tag{89}$$

$$f^{eq}_i(x,t-\Delta t) = f^{eq}_i(x,t) \tag{90}$$

$$f_i(x,t) = f_i(x,t+\Delta t) \tag{91}$$

$$\Psi^0_i = \Psi_i \tag{92}$$

$$time = time + \Delta t \tag{93}$$

Step 12: The temperature of electrons and lattices are output.
Step 13: Whether the execution time of the process is less than the end time or not is judged. If the condition is met, return to step 3, and repeat the process until the execution time is no less than the ending time; otherwise, the calculation ends.

3.2. Simulation results

The simulation results obtained by HLBM-TTM and PLBM-TTM are compared with the experimental data in the literature [36]. Fig. 3 is a comparison of the dimensionless electron temperature $\theta_e = (T_e - T_{eo})/(T_e - T_{eo})_{max}$ simulated by different models with the reflectance measured by the hot electron reflection experiment. The thermal electron reflection experiment indirectly reflects the change of the dimensionless temperature by measuring the ratio of the change value of the reflectance to the change value of the maximum reflectance. According to the Ref. [11], the relationship between the dimensionless electron temperature and the dimensionless reflectance is $\Delta T_e/(\Delta T_e)_{max} = \Delta R/(\Delta R)_{max}$.

It can be found from the Fig. 3 that the evolutionary trends obtained by HLBM-TTM and PLBM-TTM are basically consistent with the experimental data. Although, there is still a certain difference between the results of the two models, it is not too large. We calculate the dimensionless standard deviation obtained from the two models to analyze the deviation of the simulated value from the experimental value. The formula for calculating the dimensionless standard deviation is:

$$M = \frac{\sqrt{(y_c - y_e)^2/N}}{y_{e,\max} - y_{e,\min}} \tag{94}$$

where y_c is the calculation result, y_e is the experiment data, N is the number of experiment data. By calculation, we found that the M

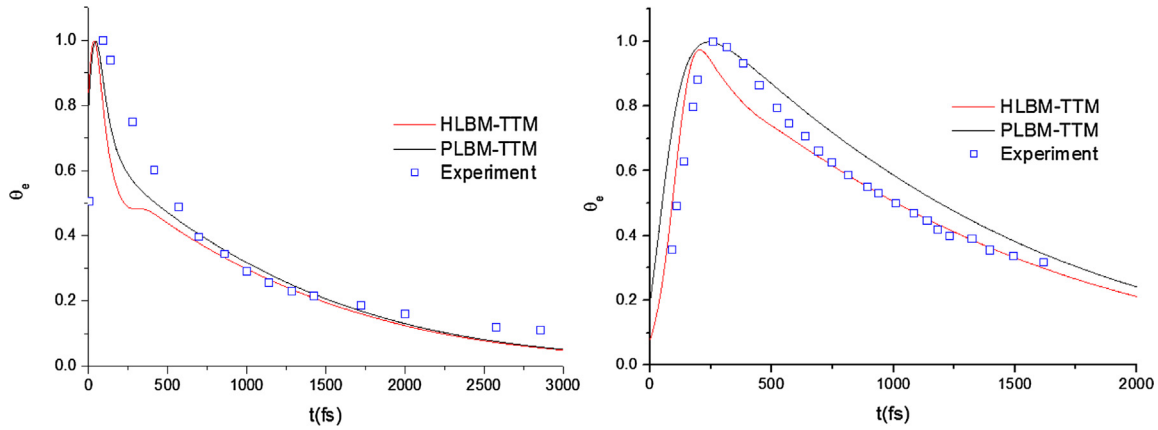

Fig. 3. The dimensionless electron temperature of the surface of the gold film obtained by the two-step model compared with the experimental data [36]. Figure (a) shows the change of the dimensionless electron temperature of the front surface of the gold film with time, and Figure (b) shows the case of the rear surface. The coordinate t is time, and the coordinate θ_e indicates the dimensionless electron temperature of the surface of the gold film. The red line is the result obtained with the HLBM proposed in this paper, the black line is the result obtained with the classic LBM, and the square patterns represent the experimental data. [L = 100 nm, J = 10 J/m^2, t_p = 96 fs, R = 0.93, δ = 20.6 nm, δ_b = 0 nm]. (For interpretation of the references to color in this figure legend, the reader is referred to the web version of this article.)

value of the front surface is 0.16 for HLBM-TTM and 0.12 for PLBM-TTM, while the *M* value of the back surface is 0.11 for HLBM-TTM and 0.20 for PLBM-TTM. From the perspective of the *M* value, the simulated value of the rear surface HLBM-TTM is more related to the experimental value, while the front surface is exactly the opposite. From Fig. 3(a), we can also see that there is a secondary peak phenomenon in the results of the HLBM-TTM simulation, the reason of that is the heat wave is reflected by the back surface and reaches the front surface again. The experiment also confirmed the existence of this phenomenon [37]. From this, the propagation velocity of the heat wave in the gold film is calculated as $v = 2L/\Delta t = 7.1 \times 10^5$ m/s, which is close to the data in the literature [36].

In addition, it should be emphasized that the electron temperatures obtained by the two models are different. The maximum electron temperatures of the front and rear surfaces obtained by HLBM-TTM were 664.0 K and 509.5 K, respectively, while those obtained by PLBM-TTM were 617.0 K and 471.8 K, respectively. This is because HLBM-TTM treats the rate of change of the source term as an additional source term, so the electron and lattice temperatures obtained by HLBM-TTM are higher than that of PLBM-TTM under the same conditions, in other words, to achieve the same temperature, the required energy value calculated by HLBM-TTM is lower than that calculated by PLBM-TTM. Based on this conclusion, we examine the advantages and disadvantages of HLBM-TTM and PLBM-TTM from the perspective of the damage threshold.

Fig. 4 shows the simulated damage thresholds of gold foil surfaces irradiated by 28 fs laser using the HLBM-TTM model and the PLBM-TTM model respectively, and the results are also compared with the data in the literature [38]. The damage threshold can be obtained by adjusting the energy density *J* of the laser so that the temperature at the front surface of the gold film reaches the melting temperature of the lattice.

Fig. 4(a) is a comparison of simulated and experimental values of a single pulse laser irradiated gold film. It can be seen from the figure that the results obtained by the HLBM-TTM simulation are

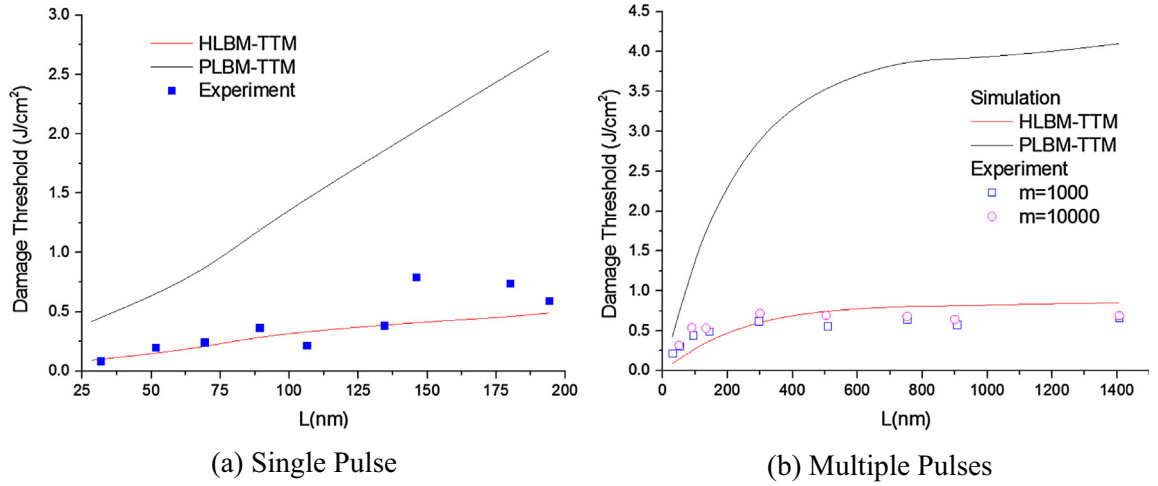

Fig. 4. The comparison between the damage threshold obtained from the two-step model and the experimental data [38]. The coordinate L is the thickness of the gold film. Figure (a) reflects the damage threshold of the single-pulse laser irradiated gold film surface, and Figure (b) reflects the multi-pulse laser case, where m represents the number of pulses. The damage threshold of the multi-pulse laser irradiated gold film surface is determined by the empirical formula (m). The red line is the result obtained with the HLBM proposed in this paper, the black line is the result obtained with the classic LBM, and the square/circular pattern represents the experimental data. [t_p = 28 fs, R = 0.98, δ = 20.6 nm, δ_b = 106 nm]. (For interpretation of the references to color in this figure legend, the reader is referred to the web version of this article.)

close to those in the literature, while the simulated values of the PLBM-TTM are much higher than the experimental values. When the thickness of the gold foil is increased, the gold foil will produce spherical protrusions, resulting in an experimental threshold being too large. In order to reduce the experimental error, the damage threshold $J_{th}(1)$ of the single-pulse laser can be obtained from the damage threshold $J_{th}(m)$ of the multi-pulse laser, and the relationship between the two is [38]

$$J_{th}(1) = J_{th}(m)/m^{\xi-1} \tag{95}$$

where $\xi = 0.87$, m is the number of pulses.

Fig. 4(b) shows the single-pulse laser impulse damage threshold obtained from the destruction threshold of a multi-pulse laser. From Fig. 4(b), it can be obtained that when m = 1000, the bulk threshold is 0.66 J/cm^2, when m = 100,000, the bulk threshold is 0.69 J/cm^2, and the bulk threshold of HLBM-TTM is 0.85 J/cm^2, the bulk threshold of PLBM-TTM is 4.1 J/cm^2.

In addition, we quantitatively check the deviation between the simulated value and the experimental value from the perspective of the M value. Calculations show that for a single pulse laser, the value of M is 0.29 for HLBM-TTM and is 1.82 for PLBM-TTM. For multi-pulse lasers, when m = 1000, the M value of HLBM-TTM is 0.38, while PLBM-TTM is 5.44; when m = 10,000, the M value of HLBM-TTM is 0.41, while PLBM-TTM is 6.22. By contrast, HLBM-TTM is closer to the experimental value.

4. Conclusion

In this paper, based on the CV model and the classic LBM, a hyperbolic lattice Boltzmann method (HLBM) was proposed. In order to verify the validity of the model, HLBM and PLBM were combined with TTM, and then were applied to simulate the non-Fourier heat transfer process of laser irradiation of gold film. The simulated values were compared with the experimental data. The results show that there is little difference between the simulated electron temperatures of two models. However, the thresholds of the two models are different. The results of the HLBM model are closer to the experimental values, and the values of the PLBM model are larger than the experimental data. Therefore, HLBM is more accurate when studying the heat transfer phenomenon with non-Fourier effect. In addition, a heat wave propagation velocity of 7.1×10^5 m/s was obtained from the simulation results of HLBM-TTM.

Conflict of interest statement

The authors declare that they have no conflict of interest to this work.

Acknowledgments

The authors gratefully acknowledge the financial support from Chinese National Natural Science Foundation under Grant No. 51476102.

References

[1] J. Fourier, The Analytical Theory of Heat, Cambridge University Press, New York, 2009.
[2] M.N. Özisik, Heat Conduction, second ed., John Wiley, New York, 1993.
[3] S.C. Mishra, H. Sahai, Analyses of non-Fourier heat conduction in 1-D cylindrical and spherical geometry – an application of the lattice Boltzmann method, Int. J. Heat Mass Transf. 55 (23–24) (2012) 7015–7023.
[4] J.I. Frankel, B. Vick, M.N. Özisik, General formulation and analysis of hyperbolic heat conduction in composite media, Int. J. Heat Mass Transf. 30 (1987) 1293–1305.
[5] C. Cattaneo, Sur une forme del'équation de la chaleur éliminant le paradoxe d'une propagation instantanée, Compte Rendus 247 (1958) 431–433.
[6] C. Cattaneo, Sulla conduzione del calore, Atti Sem. Mat. Fis. Univ. Modena 3 (1948) 83–101.
[7] P. Vernotte, Sur quelques complications possible dans les phénomènes de conduction de la chaleur, Compte Rendus 252 (1961) 2190–2191.
[8] T.-M. Chen, Numerical solution of hyperbolic heat conduction problems in the cylindrical coordinate system by the hybrid Green's function method, Int. J. Heat Mass Transf. 53 (7–8) (2010) 1319–1325.
[9] A. Kumar, S. Kumar, V.K. Katiyar, S. Telles, Phase change heat transfer during cryosurgery of lung cancer using hyperbolic heat conduction model, Comput. Biol. Med. 84 (2017) 20–29.
[10] T.Q. Qiu, C.L. Tien, Short-pulse laser heating on metals, Int. J. Heat Mass Transf. 35 (1992) 719–762.
[11] T.Q. Qiu, C.L. Tien, Heat transfer mechanisms during short-pulse laser heating of metals, J. Heat Transf. 115 (1993) 835–841.
[12] S.L. Guo, B.L. Wang, Thermal shock fracture of a cylinder with a penny-shaped crack based on hyperbolic heat conduction, Int. J. Heat Mass Transf. 91 (2015) 235–245.
[13] A.A. Mohamad, Lattice Boltzmann Method: Fundamentals and Engineering Applications with Computer Codes, Springer, London, 2011.
[14] Y. He, Y. Wang, Q. Li, Lattice Boltzmann Method: Theory and Applications, Science Press, Beijing, 2009.
[15] S. Chen, G.D. Doolen, Lattice Boltzmann method for fluid flows, Annu. Rev. Fluid Mech. 30 (1998) 329–364.
[16] X. He, L.-S. Luo, A priori derivation of the lattice Boltzmann equation, Phys. Rev. E 55 (1997) R6333–R6336.
[17] X. He, L.-S. Luo, Theory of the lattice Boltzmann method: from the Boltzmann equation to the lattice Boltzmann equation, Phys. Rev. E 56 (1997) 6811–6817.
[18] D. Raabe, Overview of the lattice Boltzmann method for nano- and microscale fluid dynamics in materials science and engineering, Modell. Simul. Mater. Sci. Eng. 12 (6) (2004) R13–R46.
[19] K.N. Premnath, J. Abraham, Three-dimensional multi-relaxation time (MRT) lattice-Boltzmann models for multiphase flow, J. Comput. Phys. 224 (2) (2007) 539–559.
[20] Y.H. Qian, D. d'Humières, P. Lallemand, Lattice BGK models for Navier-Stokes equation, Europhys. Lett. 17 (1992) 479–484.
[21] P.L. Bhatnagar, E.P. Gross, M. Krook, A model for collision processes in gases. I. Small amplitude processes in charged and neutral one-component systems, Phys. Rev. 94 (3) (1954) 511–525.
[22] J.-R. Ho, C.-P. Kuo, W.-S. Jiaung, Study of heat transfer in multilayered structure within the framework of dual-phase-lag heat conduction model using lattice Boltzmann method, Int. J. Heat Mass Transf. 46 (2003) 55–69.
[23] A. Mukherjee, A. Lahiri, S.C. Mishra, Analyses of dual-phase lag heat conduction in 1-D cylindrical and spherical geometry – an application of the lattice Boltzmann method, Int. J. Heat Mass Transf. 96 (2016) 627–642.
[24] S. Patidar, S. Kumar, A. Srivastava, S. Singh, Dual phase lag model-based thermal analysis of tissue phantoms using lattice Boltzmann method, Int. J. Therm. Sci. 103 (2016) 41–56.
[25] L. Li, L. Zhou, M. Yang, An expanded lattice Boltzmann method for dual phase lag model, Int. J. Heat Mass Transf. 93 (2016) 834–838.
[26] Y. Guo, M. Wang, Lattice Boltzmann modeling of phonon transport, J. Comput. Phys. 315 (2016) 1–15.
[27] F. Wu, W.X. Zhong, A modified stochastic perturbation method for stochastic hyperbolic heat conduction problems, Comput. Methods Appl. Mech. Eng. 305 (2016) 739–758.
[28] J. Zhao, P. Cheng, A lattice Boltzmann method for simulating laser cutting of thin metal plates, Int. J. Heat Mass Transf. 110 (2017) 94–103.
[29] J.K. Chen, W.P. Latham, J.E. Beraun, The role of electron-phonon coupling in ultrafast laser heating, J. Laser Appl. 17 (2005) 63–68.
[30] S.I. Anisimov, B.L. Kapeliovich, T.L. Perel'man, Electron emission from metal surfaces exposed to ultrashort laser pulses, Sov. Phys. JETP 39 (1974) 375–377.
[31] W. Dai, T. Niu, A finite difference scheme for solving a nonlinear hyperbolic two-step model in a double-layered thin film exposed to ultrashort-pulsed lasers with nonlinear interfacial conditions, Nonlinear Anal. Hybrid Syst. 2 (1) (2008) 121–143.
[32] J.K. Chen, D.Y. Tzou, J.E. Beraun, A semiclassical two-temperature model for ultrafast laser heating, Int. J. Heat Mass Transf. 49 (1–2) (2006) 307–316.
[33] S.I. Anisimov, B. Rethfeld, The theory of ultrashort laser pulse interaction with a metal, Proceedings of SPIE-The International Society for, Opt. Eng. 3093 (1997) 192–203.
[34] Y. Zhang, J.K. Chen, An interfacial tracking method for ultrashort pulse laser melting and resolidification of a thin metal film, J. Heat Transf. 130 (2008) 1–10.
[35] J. Huang, Y. Zhang, J.K. Chen, Ultrafast solid–liquid–vapor phase change in a thin gold film irradiated by multiple femtosecond laser pulses, Int. J. Heat Mass Transf. 52 (13–14) (2009) 3091–3100.
[36] S.D. Brorson, J.G. Fujimoto, E.P. Ippen, Femtosecond electronic heat-transport dynamics in thin gold films, Phys. Rev. Lett. 59 (17) (1987) 1962–1965.
[37] H. Wang, W. Ma, X. Zhang, W. Wang, Measurement of the thermal wave in metal films using femtosecond laser thermoreflectance system, Acta Phys. Sin. 59 (2010) 3856–3862.
[38] J. Krüger, D. Dufft, R. Koter, A. Hertwig, Femtosecond laser-induced damage of gold films, Appl. Surf. Sci. 253 (19) (2007) 7815–7819.
[39] J.K. Chen, J.E. Beraun, Numerical study of ultrashort laser pulse interactions with metal films, Numer. Heat Transf., Part A: Appl. 40 (1) (2001) 1–20.